Measuring Sigmoidality

Paul L. Rosin

Computer Science, Cardiff University
Queen's Buildings, Newport Road, PO Box 916
Cardiff CF24 3XF, Wales, UK
Paul.Rosin@cs.cf.ac.uk

Abstract. Several new shape measures are proposed for measuring the *sigmoidality* of a region (or more precisely, the region's axis). The correctness of the measures are verified on synthetic data, and then tested quantitatively on a *diatom* classification task.

1 Introduction

The analysis of form is required in many areas. However, notions of shape tend to be vague, and difficult to pin down. Scientific disciplines often provide specialised definitions of shape terms relevant to their subjects of interest. Thus, in botany there are standard descriptors for gross leaf shape, leaf base, leaf margin (i.e. boundary pattern), and so on. In computer vision a more general set of shape descriptors have been developed. Well known examples are symmetry, eccentricity, Euler number, compactness, convexity, and rectangularity [10], while more recent developments have been chirality [5], triangularity [9] and rectilinearity [13].

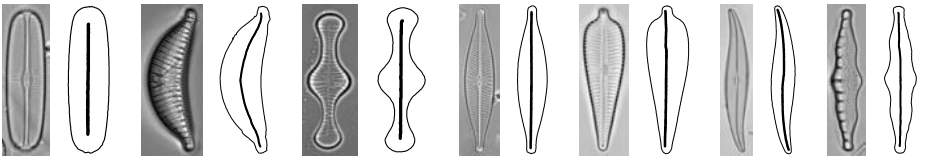

Fig. 1. Examples of diatoms shown next to their extracted contours and axes.

This paper describes a new shape descriptor for *sigmoidality*, motivated[1] by the classification of *diatoms* (see figure 1), which are unicellular algae found in water [2], and have many applications in forensics, geology, etc. There is a limited range of diatom shapes that occur, and so variations in shape between taxa can be quite subtle. While techniques such as Legendre polynomial coefficients [11] and Fourier descriptors [7] have been traditionally used for diatom shape analysis, Fischer and Bunke [4] found that incorporating additional shape descriptors like those listed above improved classification

[1] Other applications of sigmoidal shape are e.g. classification of solar active regions as eruptive/non-eruptive [1], and as a descriptor of the anatomy of bones [12].

N. Petkov and M.A. Westenberg (Eds.): CAIP 2003, LNCS 2756, pp. 410–417, 2003.

rates. Moreover, such intuitive, symbolic descriptors are closer to those currently used by biologists[2].

2 Sigmoidality Measures

The sigmoidal shape is generally described as S shaped, but there is no single precise definition. The measures described in this paper start with a tightly specified function and progress to more general sigmoidal shapes.

While shapes such diatoms are outlines of two dimensional regions, in this paper we only consider the central axis. This is extracted by applying a standard thinning algorithm [14] to the region. If the resulting axis contains vertices then the boundary is iteratively blurred until a simple axis curve is obtained. While this scheme will not work well for substantially branched shapes they are not sigmoidal in any case, and will not be considered further. Also, this paper does not consider details of the shape such as variations in the cross section along the axis, the thickness (width) of the shape, the shape of endings, etc.

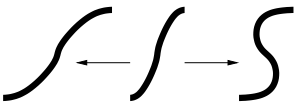

Fig. 2. Differents types of variation of a sigmoidal curve.

As shown in figure 2 stretching the shape to increase its curvature has a greater perceptual effect than stretching along its principal axis. Nevertheless, is the right hand shape really more sigmoidal then the others? The measures in this paper do not take the "fullness" of the shape into account.

2.1 Cubic Fit

For diatom classification Fischer and Bunke [4] fit a cubic polynomial and classify the shape based on the coefficient values. We also fit a cubic, but since we are focussing attention on the sigmoid shape we use $y = ax^3 + bx + c$ and miss out the x^2 term to ensure a symmetric curve is fitted. Before the least squares fitting the data is first rotated so that its principal axis lies along the X axis. The correlation coefficient ρ is used to measure the quality of fit. Since we are not expecting inverse correlation the value is truncated at zero, and so the sigmoidality measure is $S_1 = \max(\rho, 0)$. The range of all the measures described in this paper is $0 - 1$.

2.2 Generalized Gaussian Fit

Rather than fit directly to the coordinates the next approach uses the tangent angle instead. This has the advantage that apart from a simple offset of the values the angle is orientation invariant. If we plot the following sigmoid function

[2] Some examples of descriptors (with explanations) commonly used for diatom outlines are: acicular (needle), arcuate (strongly curved), clavate (club), cruciform (cross), cuneate (wedge), elliptical, lenticular (lens), linear, lunate (crescent), panduriform ('8'), sigmoid, stellate (star).

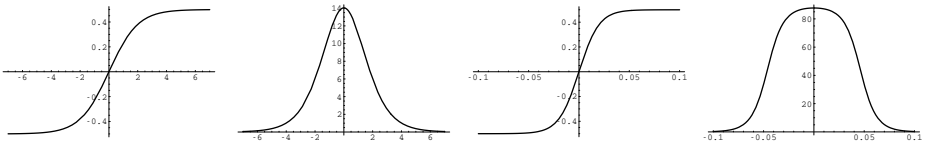

(a) $a = 1$ (b) $a = 1$ (c) $a = 100$ (d) $a = 100$

Fig. 3. Sigmoid function (a & c) and tangent angle (b & d).

$$0.5 - \frac{1}{1 + e^{ax}}$$

we see (figure 3a&c) that increasing the value of a sharpens the transition between the middle section and the outer arms. The corresponding tangent angle looks somewhat Gaussian, but is flattened as the sigmoid function becomes sharper. The shape of the tangent angle plot can be modelled well by the Generalized Gaussian distribution. The probability density function is given by

$$p(x) = \frac{vn(v,s)}{2\Gamma(1/v)} e^{-[n(v,s)|x|]^v} \qquad \text{with} \qquad n(v,s) = \sqrt{\frac{\Gamma(3/v)}{\Gamma(1/v)}}/s$$

where v is a shape parameter controlling the peakiness of the distribution. Since the maximum likelihood estimate requires solving a highly nonlinear equation we use Mallat's method [6] for approximating the solution which is computationally simpler. First the mean absolute value and variance of the data x_i are matched to the Generalized Gaussian. If $m_1 = \frac{1}{n}\sum_{i=1}^{n} |x_i|$ and $m_2 = \frac{1}{n}\sum_{i=1}^{n} x_i^2$ then

$$v = F^{-1}\left(\frac{m_1}{\sqrt{m_2}}\right) \qquad \text{where} \qquad F(\alpha) = \frac{\Gamma(2/\alpha)}{\sqrt{\Gamma(1/\alpha)\Gamma(3/\alpha)}}.$$

In practise, values of $F(\alpha)$ are precomputed, and the inverse function determined by a look-up table with linear interpolation. Finally, the tangent angle is scaled so that the area under the curve sums to one. Again the error of fit was determined using the correlation coefficient, $S_2 = \max(\rho, 0)$.

2.3 Curvature Analysis

A characteristic of the sigmoid is its single, central point of inflection. For perfect, clean data its presence would be easy to test, but in practise, with real data the sensitivity of curvature estimation to noise makes this hopeless. Although the data could be smoothed to eliminate false inflections the parameter for the degree of smoothing would be crucial. Instead of identifying zero crossings of curvature we check the overall distribution of curvature values along the curve. The curvature at each point is estimated as κ_i using kernels of the Gaussian function and its first two derivatives. Since the curvature will be integrated along the curve and the number of zero crossings is not critical then the value for the spread of the Gaussian is not critical either. Separating the positive and negative curvature values as

$$\kappa_i^+ = \begin{cases} 0 & \text{if } \kappa_i < 0 \\ \kappa_i & \text{otherwise} \end{cases} \qquad \kappa_i^- = \begin{cases} 0 & \text{if } \kappa_i > 0 \\ -\kappa_i & \text{otherwise} \end{cases}$$

then the positive and negative curvature values are summed over the curve to the left and right respectively of the midpoint m. In addition the total curvature is computed for normalisation purposes:

$$A^+ = \sum_{i=1}^{m} \kappa_i^+ \qquad A^- = \sum_{i=m}^{n} \kappa_i^- \qquad S = \sum_{i=1}^{n} |\kappa_i| \,.$$

The sections of positive and negative curvature should be restricted to either side of the inflection point and so the quantity $A^+ + A^-$ should be large. Also, the amount of positive curvature on the left should equal the (absolute) value of the negative curvature on the right, and the discrepancy is measured by $|A^+ - A^-|$. These values are scaled to lie in the range $0 - 1$ and combined using a product to obtain the following measure

$$S_3 = \left[1 - \frac{2\,(A^+ + A^-)}{S}\right] \left[1 - \frac{|A^+ - A^-|}{S}\right].$$

To cope with the curve bending in either direction it is analysed both for κ_i and $-\kappa_i$, and the larger of the two values returned.

Figure 4 shows several examples of curvature plots in which the quantities A^+ and A^- are shaded dark and light gray respectively. Only the first example gets a score of one and the remainder are assigned zero either due to the first (b and c) or the second term (d).

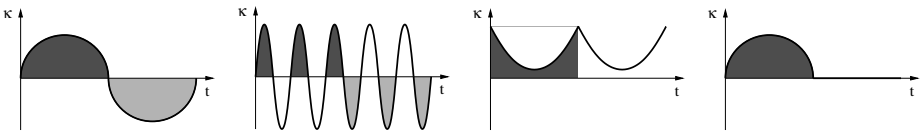

(a) $S_3 = 1 \times 1$ (b) $S_3 = 0 \times 1$ (c) $S_3 = 0 \times 0.5$ (d) $S_3 = 1 \times 0$

Fig. 4. Curvature plots with the shaded regions corresponding to A^+ and A^-.

2.4 Convex Hull Method

The final method splits the curve in two at its midpoint, and the convex hull of each section is determined. Next, each section is traversed from the midpoint to the other end of the curve, and the areas to the left and right sides of the curve are calculated. If these are L_1 and R_1 for section 1, and likewise for section 2, then ideally $L_1 = L_2$ and $R_1 = R_2 = 0$ (or the equivalent with L and R switched). This corresponds to the two sections being convex on opposite sides, and partially enclosing areas of similar sizes. Like S_3, the precise shape of the curve is immaterial. An appropriate normalised measure is

$$S_4 = \left(1 - \frac{|L_1 - L_2|}{L_1 + L_2}\right) \left(1 - \frac{R_1 + R_2}{L_1 + L_2 + R_1 + R_2}\right).$$

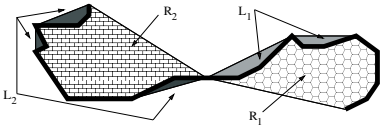

Fig. 5. For the given axis (in bold) the convex hull is determined for each half. The areas to the left/right of each axis section (when traversing from the axis midpoint) are hatched/shaded.

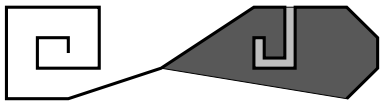

Fig. 6. The areas for the left hand spiral section cannot be calculated, although the other section is not problematic.

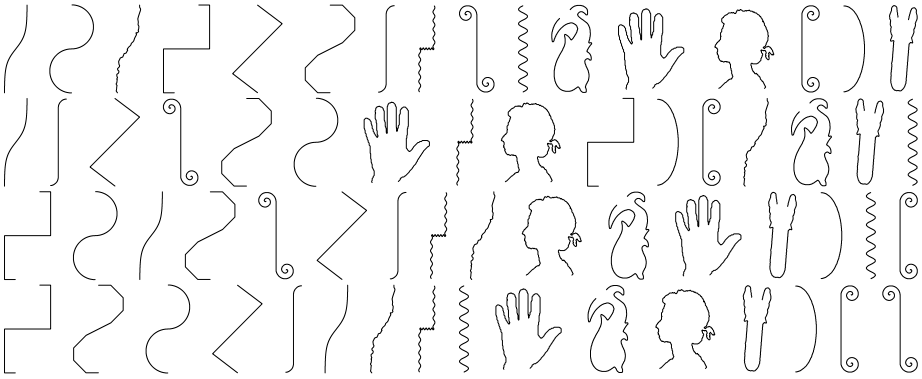

Fig. 7. In each row the curves are ranking in decreasing order according to S_1, S_2, S_3, S_4 respectively.

To be able to determine the areas this method assumes that the endpoints are vertices in the convex hull. Otherwise, problems arise such as shown in the left hand section in figure 6.

3 Experimental Results

3.1 Contour Example

The four measures are first tested on some synthetic curves and a miscellaneous selection of other curves. The curves are shown in figure 7, ranked in descending order of sigmoidality. All measures do reasonable well, generally assigning high scores to sigmoidal curves. Also, as already noted, S_4 cannot cope with the spiral sinusoid.

Examining the distribution of the sigmoidal measures (figure 8) it can be seen that S_2, S_3 and S_4 all correctly give close to peak responses for the first six noise free sinusoids. Due to its more restrictive model S_1 shows a drop-off.

3.2 Diatom Example

The second experiment applies the shape measures to classify diatoms. The mixed genera set from the ADIAC project was used, consisting of 808 contours covering 38 taxa. Out

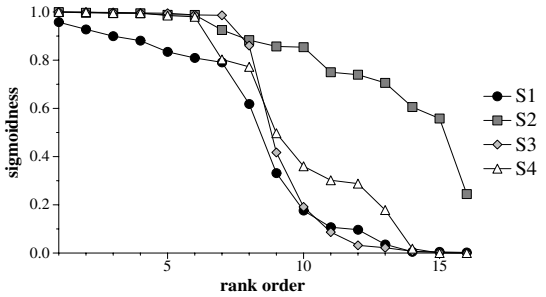

Fig. 8. Distribution of values calculated by sigmoidality measures for data shown in figure 7.

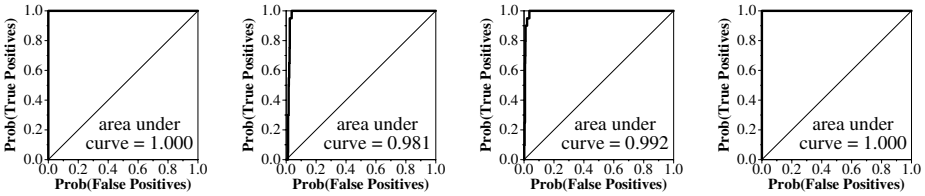

(a) S_1 (b) S_2 (c) S_3 (d) S_4

Fig. 9. ROC curves for identification of *Gyrosigma acuminatum* diatoms.

of the 38 taxa (classes) there is only one with a sigmoidal shape: *Gyrosigma acuminatum*. Between 20 and 29 examples of each taxa were present.

For each sigmoidal shape measure, as well as some standard shape descriptors, their discriminating power was calculated for identifying *Gyrosigma acuminatum* diatoms against all other diatoms (i.e. a two class problem). Receiver operating characteristic (ROC) curves were generated, showing the trade-offs between the amount of true and false positives for all the different threshold values – see figure 9. The area under the ROC curve corresponds to the probability of a correct decision in a two-interval, forced choice task [3], and is listed in table 1. As expected, the sigmoidal shape measures do a good job of discriminating the sigmoidal diatoms, and are clearly better at the task than the other shape descriptors.

Next, classification of the full set of 38 class labels was performed using Murthy *et al.*'s oblique decision trees [8], the set of 15 non-sigmoidal shape descriptors given in table 1, plus one sigmoidal shape measure at a time. Leave-one-out cross validation produced the classification accuracies in table 2 [3]. S_1 was found to perform best, (perhaps since *Gyrosigma acuminatum* have a consistent, regular sigmoidal shape) improving classification accuracy by 3%, while S_2 performs worst. Overall, there seems to be a small but consistent improvement in classification accuracy when one or other of the

[3] Fischer and Bunke [4] reported better accuracies than ours (in excess of 90%). However, they used diatom specific features (e.g. 10 descriptors for valve endings) as well as internal textural details ("ornamentation"). Moreover, by applying bagging they further increased the performance of the decision tree classifiers.

Table 1. Areas under ROC curves for identification of *Gyrosigma* diatoms.

Sigmoidality measures				
method	S_1	S_2	S_3	S_4
area	1.000	0.981	0.992	1.000
Geometric primitives				
method	circularity	ellipticity	rectangularity	triangularity
area	0.142	0.180	0.386	0.060
Classical measures				
method	aspect ratio	compactness	convexity	eccentricity
area	0.203	0.881	0.112	0.818
RTS Moment invariants				
method	ϕ_1	ϕ_2	ϕ_3	ϕ_4
area	0.826	0.825	0.374	0.437
Affine Moment invariants				
method	I_1	I_2	I_3	
area	0.820	0.689	0.708	

Table 2. Diatom classification success rate for all 38 taxa. The columns show which sigmoidality measure was used in addition to the set of general shape descriptors.

S_1	S_2	S_3	S_4	none
78.47	75.62	76.36	77.72	75.25

sigmoidal measures (apart from S_2) are combined with the other descriptors, confirming that sigmoidality does provide some useful discriminating power in this application.

4 Conclusions

Four measures for computing the sigmoidality of a shape have been described. All have linear computational complexity and are straightforward to implement. From the experiments reported in this paper it is not possible to choose any one method as the best. All performed reasonably; S_2 fared worst, but the others produced similar levels of performance considering both the two-way and 38-way diatom classification tasks. The latter three also showed that an improvement in classification could be achieved over using just standard shape descriptors. Future work will investigate testing and comparing the measures over a wider range of applications.

Acknowledgements

The diatom data was kindly provided by the ADIAC project; CEC contract MAS3-CT97-0122.

References

1. R.C. Canfield, H.S. Hudson, and D.E. McKenzie. Sigmoidal morphology and eruptive solar activity. *Geophysical Research Letters*, 26(6):627–630, 1999.
2. J.M.H. du Buf and M.M. Bayer, editors. *Automatic Diatom Identification*. World Scientific, 2002.
3. J.P. Egan. *Signal Detection Theory and ROC Analysis*. Academic Press, 1975.
4. S. Fischer and H. Bunke. Identification using classical and new features in combination with decision tree ensembles. In J.M.H. du Buf and M.M. Bayer, editors, *Automatic Diatom Identification*, pages 109–140. World Scientific, 2002.
5. Y. Hel-Or, S. Peleg, and D. Avnir. Characterization of right handed and left handed shapes. *Computer Vision, Graphics and Image Processing*, 53(2):297–302, 1991.
6. S.G. Mallat. A theory for multiresolution signal decomposition: the wavelet representation. *IEEE Transactions on Pattern Analysis and Machine Intelligence*, 11(7):674–693, 1989.
7. D. Mou and E.F. Stoermer. Separating Tabellaria (Bacillariophyceae) shape groups: A large sample approach based on Fourier descriptor analysis. *J. Phycology*, 28:386–395, 1992.
8. S.K. Murthy, S. Kasif, and S. Salzberg. System for induction of oblique decision trees. *Journal of Artificial Intelligence Research*, 2:1–33, 1994.
9. P.L. Rosin. Measuring shape: Ellipticity, rectangularity, and triangularity. *Machine Vision and Applications*, forthcoming.
10. M. Sonka, V. Hlavac, and R. Boyle. *Image Processing, Analysis, and Machine Vision*. Chapman and Hall, 1993.
11. E.F. Stoermer and T.B. Ladewski. Quantitative analysis of shape variation in type and modern populations of Gomphoneis herculeana. *Nova Hedwigia*, 73:347–386, 1982.
12. A.R. Tolat, J.K. Stanley, and I.A. Trail. A cadaveric study of the anatomy and stability of the distal radioulnar joint in the coronal and transverse planes. *J. Hand Surg. [Br]*, 21:587–594, 1996.
13. J. Žunić and P.L. Rosin. A rectilinearity measurement for polygons. *IEEE Transactions on Pattern Analysis and Machine Intelligence*, forthcoming.
14. T.Y. Zhang and C.Y. Suen. A fast parallel algorithm for thinning digital patterns. *Comm. ACM*, 27(3):236–240, 1984.